RESEARCH ACTIVITIES II
Department of Molecular Structure

II-A Development of Near-Field Dynamic Spectroscopy and Application to Mesophase Systems

Recent developments in ultrashort pulsed lasers have made ultrafast spectroscopy a mature technique for analyzing dynamic behavior of molecular systems. As for spatial resolution, near-field optical microscopy, which enables spatial resolution beyond the diffraction limit of light, shows remarkable progress in technology in these days. Combination of these advanced optical technologies may offer a direct probe of molecular dynamical processes in mesoscopic systems. It may bring essential and basic knowledge for analyzing origins of characteristic features and functionalities of mesophase systems. We are constructing an apparatus for near-field dynamic spectroscopy with femtosecond temporal resolution and nanometer spatial resolution. Preliminary experimental results are presented here.

II-A-1 Development of an Ultrafast Near-Field Spectroscope and Observation of Dynamic Processes in GaAs Crystal

IMURA, Kohei; OKAMOTO, Hiromi

We have developed an instrument, where a fs pump-probe technique is combined with a scanning near-field optical microscope having a 100-nm spatial resolution, for the purpose of obtaining information on spatially resolved molecular dynamics. We have examined the performance of our instrument and feasibility of applications to the studies of molecular dynamics by using a GaAs crystal.

Experimental set-up consists of an excitation light source, a near-field microscope, and detection systems. The output from a mode-locked Ti:sapphire laser (λ = 780 nm, ~100 fs pulse duration) is split into two beams. The beams are collinearly combined again into one beam after one beam passes through a motorized optical delay line. Positive group velocity dispersion arising from a long optical fiber (for a near-field probe) is pre-compensated by a grating-prism pulse stretcher before the optical beam is coupled to the cleaved end of the fiber. The other end of the fiber has been fabricated as a near-field probe. The near-field probe (commercial) is tapered and Au metal coated, and has an aperture (~100 nm) at the tip. The aperture probe is used to illuminate the sample, and also to collect photoluminescence (PL) from the sample. The PL is detected either by a CCD after dispersed by a monochromator or by a photomultiplier tube after passing through optical filters. To obtain PL images, the sample is raster-scanned beneath the tip, and a sample-tip distance is regulated at ~10 nm by the shear force feedback mechanism. This feedback signal also gives topographic image of the sample.

We have measured the excitation laser power (P) dependence of the PL intensity (I) from the GaAs crystal around 870 nm, and have found a relationship as $I \propto P^{1.5}$. This finding indicates two-photon process involved in the PL. We have performed time-correlated measurements for the two-photon PL from GaAs crystal at ~870 nm. In Figure 1, the PL intensity is plotted against the delay time between the two optical beams. Except for the region around the origin of the delay time, where it shows an interferometric pattern (not shown in Figure 1), a relatively slow decrease of the intensity with delay time is observed. This plot gives information essentially equivalent to that obtained by the time-resolved absorption correlation method (*i.e.*, dynamics in the one-photon excited state). A relaxation time constant 52 ps is obtained by assuming a single exponential decay. The background PL with no delay time dependence is due to the two-photon PL arising from each optical pulse, as well as a single photon inter-band transition.

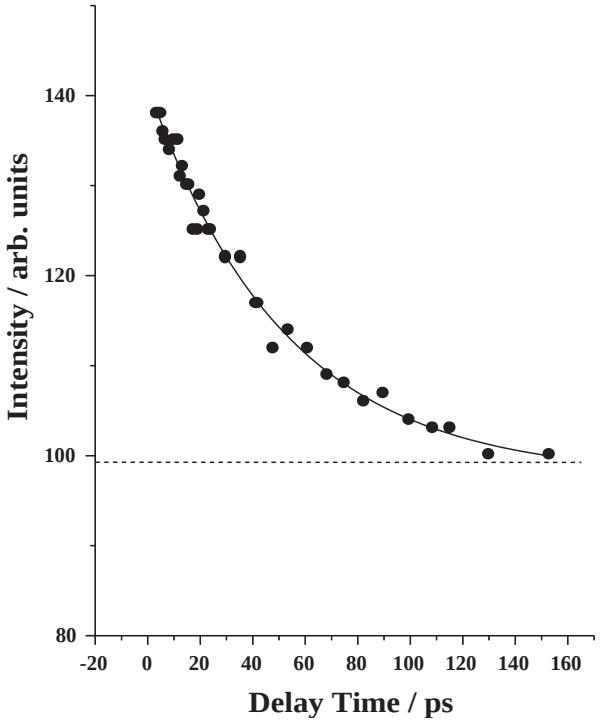

Figure 1. Near-field time-correlated PL signal of GaAs crystal.

II-A-2 Near-Field Autocorrelation Measurements of Femtosecond Light Pulses at a Tip of a 100-nm Apertured Probe by Two-Photon-Induced Photoconductivity

NAGAHARA, Tetsuhiko; IMURA, Kohei; OKAMOTO, Hiromi

In ultrafast pump-probe experiments, it is essential to characterize temporal profiles of the pump and probe light pulses. The technique most commonly used for that purpose is based on a Michelson-type autocorrelator combined with phase-matched second harmonic generation (SHG) in nonlinear crystals. For ultrafast experiments under scanning near-field optical microscopes (SNOM), however, such a conventional autocorrelation technique with the SHG crystal is not practical because of unsatisfied phase-matching condition and low radiation energy emerging from the apertured fiber probe. By the use of two-photon-induced photoconductivity in semiconductors, autocorrelation measurements under SNOM are possible. Autocorrelation trace of 470 fs full width at half maximum (FWHM) was reported in SNOM geometry.[1] Utilizing this technique, time resolution of our newly developed femtosecond SNOM apparatus has been measured.

The photocurrent output of a GaAsP diffusion type photodiode was detected by a lock-in amplifier. The signal has been confirmed to be of quadratic response (Figure 1A). Femtosecond light pulses were obtained from a mode-locked Ti:sapphire laser (pulse duration <100 fs). Normal group velocity dispersion arising from the optical fiber for the apertured probe was pre-compensated by a grating pair. Figure 1B shows the autocorrelation trace of the Ti:sapphire laser pulses at a tip of a 100-nm apertured fiber probe. The FWHM obtained is ~100 fs, which indicates that dispersion by the fiber is successfully pre-compensated in our apparatus. The spatial uniformity of the detector sensitivity was also examined (Figure 1C), by scanning the probe with the distance between the detector surface and the probe tip kept constant. There was no detectable correlation between the topographic structure and the photocurrent image. The dark spots found in Figure 1C may be ascribed to defect sites of the semiconductor.

Reference

1) W. Schade, J. Preusser, D. L. Osborn, Y. Y. Lee, J. deGouw and S. R. Leone, *Opt. Commun.* **162**, 200 (1999).

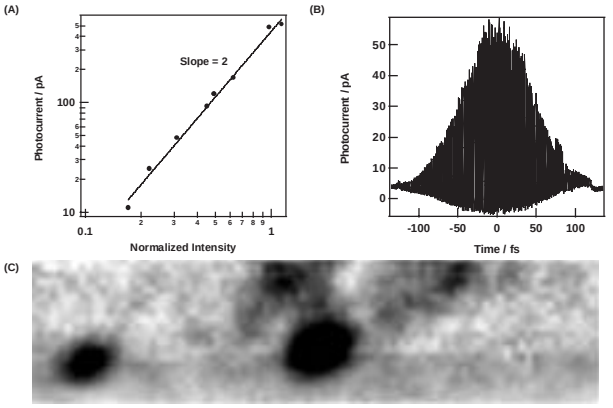

Figure 1. (A) Peak diode current as a function of normalized incident pulse energy. Solid line shows a quadratic fit to the data. (B) Autocorrelation signal obtained at the tip of the 100-nm apertured probe. (C) Spatial image (area size: 5 μm × 1.25 μm) of photocurrent.

II-A-3 Structure and Photophysics of PIC J-Aggregates Studied by Scanning Near-Field Optical Microscopy

IMURA, Kohei; NAGAHARA, Tetsuhiko; OKAMOTO, Hiromi

Molecular assemblies such as J-aggregates have received much attention over the past decades because of their characteristic optical properties. The J-aggregates are characterized by a strong and sharp optical absorption band, called J-band, which is red-shifted with respect to the monomer absorption. It has been interpreted that the strong absorption arises from the interactions between the monomeric molecular transition dipoles. Intermolecular interaction between dipoles causes the coherent delocalization of excitons over an aggregate. Pseudoisocyanine (PIC) dye is known as a typical molecule which forms a J-aggregate. Barbara and co-workers[1),2)] have studied PIC J-aggregates by scanning near-field optical microscopy. We have also observed structures and photophysics of PIC J-aggregates to examine performance of the scanning near-field microscope we have constructed recently.

PIC J-aggregate was prepared in PIC-PVS (polyvinylsulfate) hot solution and spin coated onto a substrate (cover glass). Spin-coated J-aggregate was excited by the second harmonic (527 nm) output of Nd:YLF laser through a sub-wavelength-sized (100 nm) aperture probe. J-band fluorescence from the aggregate (~575 nm) was collected by a high NA objective lens and detected by a photomultiplier tube. In order to investigate structures of the J-aggregate, the sample is scanned beneath the probe by keeping the sample-probe distance constant. Fluorescence and simultaneously obtained topographic images proved that produced J-aggregates have fibrous structures. The aggregates are longer than 10 μm in length, 10–150 nm in width, and 1–50 nm thick, depending on the sample preparation condition. We have also investigated the polarization characteristics of the near-field fluorescence for the fibrous J-aggregates. It has been found that the fluorescence from the J-aggregate depends little on the polarization of the excitation light. On the other hand, polarization of the fluorescence is strongly correlated to the fiber direction as seen in Figures 1(c) and (d). The latter observation indicates that the direction of transition dipole for the J-band fluorescence lies along the long axis of the J-aggregate as reported before.[2)] Time-resolved spectroscopic studies of the aggregates are under progress.

References

1) D. A. Higgins and P. F. Barbara, *J. Phys. Chem.* **99**, 3 (1995).
2) D. A. Higgins, P. J. Reid and P. F. Barbara, *J. Phys. Chem.* **100**, 1174 (1996).

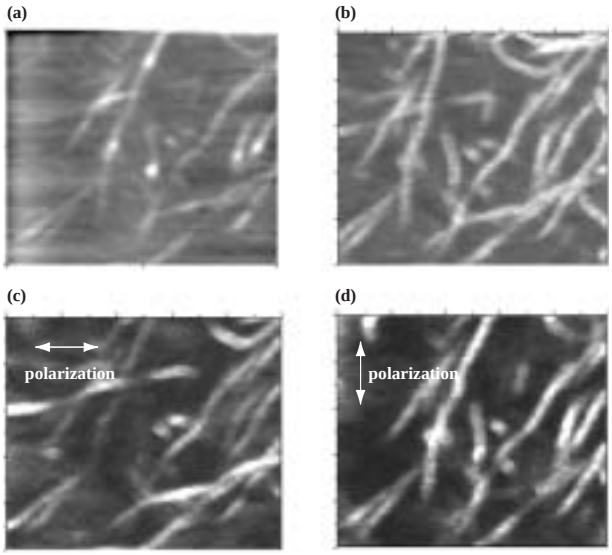

Figure 1. Observed images of J-aggregates (scan range 5 μm × 5 μm). (a) Shear-force topography. (b) Unpolarized fluorescence image. (c) Horizontally and (d) vertically polarized fluorescence images.

II-B Laser Cooling and Trapping of Metastable Helium Atoms

In the past two decades, extensive developments have occurred in the laser cooling and trapping of neutral atoms, with many workers reporting the application of these techniques to such diverse atomic species as alkali atoms, alkali earth atoms, and rare gas atoms. Among these, the helium atom is unique on account of its small mass, simple energy level structure, and easy availability in two isotopic forms (^{3}He and ^{4}He) of differing quantum statistics. For this reason, we have been studying the laser cooling and trapping of helium atoms.

II-B-1 New Design for Efficient Magneto-Optical Trapping of Metastable Helium Atoms

MORITA, Norio

The first step for Bose-Einstein condensation of metastable helium atoms is to realize an efficient magneto-optical trap (MOT). For this purpose, it is especially important to increase the intensity of a metastable atomic beam for loading the atoms into a MOT. To obtain an intense metastable beam, it is necessary to collimate the beam as tightly as possible. In our new apparatus, the metastable beam is collimated using a chain of corner cube prisms and laser beams with two detuned frequencies; the length of the collimation region along the atomic beam is 300 mm. The far detuned laser light can collimate more diverging atoms and the less detuned one collimates less diverging atoms. From our simulation, it is confirmed that this system can collimate an initial divergent beam with a spread of ±70 mrad at a velocity of 850 m/s into an almost collinear beam.

After deceleration through the Zeeman cooling process, the collimated metastable beam at a velocity of 150 m/s is deflected by an angle of 30 degrees using laser beams with curved wavefront, which are produced by a pair of cylindrical mirrors. The metastable beam is then introduced to a small glass cell, in which the atoms are trapped and further cooled for the Bose-Einstein condensation. Due to this deflection of the metastable beam, the trapping region is prevented from the attack of the intense ground state helium beam, and we can expect the longer lifetime of the trap.

While these atomic loading system is designed for a metastable beam source cooled with liquid nitrogen, we are preparing another system for liquid-helium-cooled metastable beam source in order to obtain a further intense metastable beam. Experiments with these systems are now in progress.

II-C Spectroscopic Studies on Atoms and Ions in Liquid Helium

Atoms and ions in liquid helium are known to reside in bubble-like cavities due to the Pauli repulsive force between electrons. Physical properties of these exotic surroundings are determined by the potential energy of the impurity-He$_n$ system, the surface tension energy of the liquid helium, and the pressure-volume work. Spectroscopic studies of such impurity atoms and ions in liquid helium are expected not only to give information on the structure and dynamics of the bubbles but also to contribute to the study on the property of superfluid liquid helium.

II-C-1 Laser Spectroscopy of Eu Atoms in Liquid ^{3}He and ^{4}He

MORIWAKI, Yoshiki[1]; MORITA, Norio
([1]Toyama Univ.)

Spectra of impurity atoms in liquid helium often explicitly reflect physical properties of the liquid. In this meaning, it may especially be interesting to investigate the spectral difference between impurity atoms in liquid ^{3}He and ^{4}He, because each liquid has much different physical properties at a temperature below the lambda point (2.1 K); for example, the fluidity is super and normal for ^{4}He and ^{3}He, respectively, the dispersion relation is well determined for ^{4}He but not well for ^{3}He, and the number density and surface tension are much different between ^{3}He and ^{4}He.

In this study we have experimentally obtained some spectra of Eu atoms in liquid ^{4}He and ^{3}He. Excitation spectra of the $4f^6(^7F)5d6s^2\ ^8F_{7/2} \leftarrow 4f^7 6s^2\ ^8S_{7/2}$ transition at several temperatures are shown in Figure 1. With decreasing the temperature, very sharp spectra appear and their intensities both in liquid ^{4}He and ^{3}He are increased. It is reasonable to interpret these sharp spectra as zero phonon lines, because the interaction between He atoms and the inner-shell electron excited in Eu atom is quite weak during the transition. Side bands are also seen, but they are only in the upper energy side for both liquid ^{4}He and ^{3}He. The shift of the zero phonon line and the spectral width of the side band are both smaller for liquid ^{3}He than for ^{4}He. This fact can be understood by the difference in the number density and surface tension between ^{4}He and ^{3}He: smaller number density and surface tension of ^{3}He result in the smaller spectral shift and width. An especially interesting spectral feature is that, only for liquid

^{4}He, some peaks other than the phonon side bands are also seen at a temperature of 1.1 K, but they are not seen for ^{3}He. It is quite possible that these are roton or maxon spectra of liquid ^{4}He. Further investigation is now in progress.

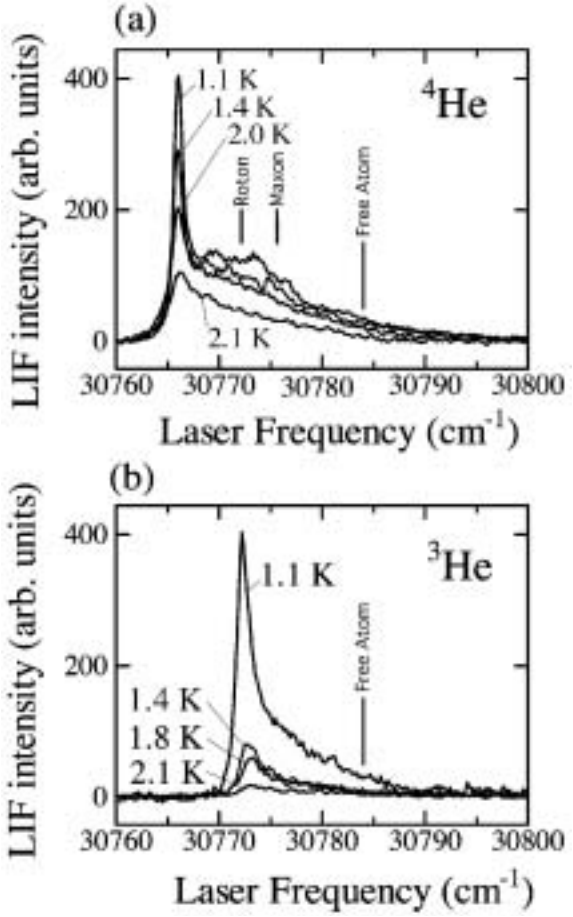

Figure 1. Excitation spectra of the $4f^6(^7F)5d6s^2\ ^8F_{7/2} \leftarrow 4f^76s^2\ ^8S_{7/2}$ transition of Eu atoms in (a) liquid ^{4}He and (b) liquid ^{3}He at several temperatures.

II-D Electron Transfer Regulation in Tetraheme Cytochromes *c*

Tetraheme cytochromes *c* are involved in the anaerobic energy metabolism. Cytochrome c_3 (cyt c_3) is an electron transport protein working in strictly anaerobic sulfate-reducing bacteria. This is a small (M. W. ≈ 14,000) soluble protein and shows very low redox potentials (typically, –240 ~ –357 mV *vs.* NHE). Small tetraheme cytochrome *c* (ST cyt *c*) is found in facultative anaerobes of *Shewanella* species and is the smallest tetraheme cytochrome (M. W. ≈ 12,000). The four hemes in ST cyt *c* is arranged in a chain-like manner in contrast to the cyclic heme architecture in cyt c_3. The major aims of this project is to elucidate the mechanism of the regulation of the electron transfer in tetraheme cytochromes *c* on the basis of tertiary structure and heme architecture. For this purpose, we are characterizing two different cytochromes mentioned above by NMR and electrochemistry. Since porphyrin is one of important elemental materials in nano-science, elucidation of the function of particular heme architectures would also contribute to this field.

II-D-1 Redox-Coupled Conformational Alternations in Cytochrome c_3 from *D. vulgaris* Miyazaki F on the Basis of its Reduced Solution Structure

HARADA, Erisa[1,2]; FUKUOKA, Yuki[2]; OHMURA, Tomoaki[3]; FUKUNISHI, Arima[2]; KAWAI, Gota[4]; FUJIWARA, Toshimichi[1]; AKUTSU, Hideo[1]
([1]Osaka Univ.; [2]Yokohama Natl. Univ.; [3]Mitsubishi Heavy Ind.; [4]Chiba Inst. Tech.)

[*J. Mol. Biol.* **319**, 767 (2002)]

Heteronuclear NMR spectroscopy was performed to determine the solution structure of ^{15}N-labeled ferrocytochrome c_3 from *Desulfovibrio vulgaris* Miyazaki F (*Dv*MF). Although the folding of the reduced cytochrome c_3 in solution was similar to that of the oxidized one in the crystal structure, the region involving hemes 1 and 2 was different. The redox-coupled conformational change is consistent with the reported solution structure of *Desulfovibrio vulgaris* Hildenborough ferrocytochrome c_3, but is different from those of other cytochromes c_3. The former is homologous with *Dv*MF cytochrome c_3 in amino acid sequence. Small displacements of hemes 1 and 2 relative to hemes 3 and 4 were observed. This observation is consistent with the unusual behavior of the 2^1CH_3 signal of heme 3 reported previously. As shown by the ^{15}N relaxation parameters of the backbone, a region between hemes 1 and 2 has more flexibility than the other regions. The results of this work strongly suggest that the cooperative reduction of hemes 1 and 2 is based on the conformational changes of the C-13 propionate of heme 1 and the aromatic ring of Tyr43, and the interaction between His34 and His35 through covalent and coordination bonds. Furthermore, it turned out that the unusual conformational distortion is involved in the attachment of heme 2. This will be associated with the unique structural properties of heme 2 in cytochromes c_3.

II-D-2 A Role of the Aromatic Ring of Tyr43 in Tetraheme Cytochrome c_3 from *Desulfovibrio vulgaris* Miyazaki F

OZAWA, Kiyoshi[3]; YASUKAWA, Fumiko[3]; TAKAYAMA, Yuki[2]; KUMAGAI, Jiro[3]; OHMURA, Tomoaki[4]; CUSANOVICH, Michael A.[5]; TOMIMOTO, Yusuke[6]; OGATA, Hideaki[6]; HIGUCHI, Yoshiki[6]; AKUTSU, Hideo[1]
([1]IMS and Osaka Univ.; [2]Osaka Univ.; [3]Yokohama Natl. Univ.; [4]Mitsubishi Heavy Ind.; [5]Unv. Arizona; [6]Kyoto Univ.)

A novel *c*-type multiheme cytochrome overproduction system has been used to prepare large quantities of *Desulfovibrio vulgaris* Miyazaki F cytochrome c_3 and two mutations of the highly conserved aromatic residue, Tyr43. Tyrosine 43 is positioned parallel to the fifth heme axial ligand, His34, of heme 1 in the tetraheme cytochrome c_3. The macroscopic and microscopic formal redox potentials of Y43L and Y43F cytochromes c_3 were determined by differential pulse polarography and ^{1}H-NMR. Although the replacement of tyrosine with leucine increased all the redox potentials, the phenylalanine mutation generally decreased them. This strongly suggests that the aromatic ring at this position is important for maintenance of the extremely low redox potentials of cytochrome c_3. The effect of the leucine and phenylalanine mutations on the interacting potential between heme 1 and heme 2 shows that the aromatic ring is also involved in the cooperative reduction of these hemes. Furthermore, temperature dependent linewidth broadening in partially reduced samples established that the aromatic ring at position 43 participates in the control of the kinetics of intramolecular electron exchange. The rate of reduction of Y43L cytochrome c_3 by 5-deazariboflavin semiquinone under partially reduced conditions was significantly different from that of the wild-type in the last stage of the reduction, supporting the involvement of Tyr43 in regulation of reduction kinetics.

II-D-3 A Directional Redox-Regulator Based on the Heme-Chain Architecture in the Small Tetraheme Cytochrome *c* from *Shewanella oneidensis*

HARADA, Erisa[2]; KUMAGAI, Jiro[3]; OZAWA, Kiyoshi[3]; IMABAYASHI, Shinichiro[3]; TSAPIN, Alexandre S.[4]; NEALSON, Kenneth H.[4]; MEYER, Terrance E.[5]; CUSANOVICH, Michael A.[5]; AKUTSU, Hideo[1]
([1]IMS and Osaka Univ.; [2]Osaka Univ.; [3]Yokohama

Natl. Univ.; [4]Cal. Inst. Tech.; [5]Unv. Arizona)

[*FEBS Lett.* in press]

The macroscopic and microscopic redox potentials of the four hemes of the small tetraheme cytochrome *c* (STC) from *Shewanella oneidensis* were analyzed. The macroscopic potentials range from –248 to –138 mV, which are higher than those of *D. vulgaris* cytochrome c_3. The microscopic redox potentials show that the order of reduction is from hemes in the C-terminal domain (hemes 3 and 4) to the N-terminal domain (heme 1), showing the polarization of the tetraheme chain during the reduction. This makes heme 4 the most efficient electron delivery site. The redox characteristics of this heme architecture fit to multistep reduction of other redox centers through either heme 3 or heme 4. This mechanism could successfully elucidate the reduction mechanism of the flavin in fumarate reductase (flavocytochrome *c*). The characteristics of STC are completely different from those of a cyclic heme arrangement in cytochrome c_3. For the first time, the important role of the heme arrangement in a multiheme protein was brought to light.

II-E Studies on Higher-Order Gaussian Light Beams

II-E-1 Simple Generation of Higher-Order Gaussian Beams and the Application to Spectroscopy

SASADA, Hiroyuki
(IMS and Keio Univ.)

Recently optical vortices have attracted considerable attentions because of the phase singularity and the characteristic intensity distribution. In particular, the dark region is very useful to trap and guide cold atoms provided by laser cooling.[1)] Several methods of generating the optical vortices have been reported so far, but their efficiencies are rather low.

Last year we demonstrated a simple and efficient generation of optical vortices using glass plates and an astigmatic mode converter. However, the phase jump introduced by the glass edge is so sharp that the generated beam consists of many higher-order Gaussian modes, and hence has too many vortices.

To overcome these difficulties, we have demonstrated a novel method using an interferometer. A Gaussian beam is first split into two beams by a polarizing beam splitter. Each beam is reflected once by a mirror, then overlapped again with a small misalignment at a beam splitter. A λ/2-wave plate is located in an arm to allow the two beams to interfere. The phase difference between two arms is adjusted so that the two beams have an opposite phase against each other at an output port. The resultant beam is very close to the HG_{10} mode (HG: Hermite-Gaussian). It is further converted into the LG_{01} mode (LG: Laguerre-Gaussian) with an optical vortex by an astigmatic mode converter. This method is also extended to generate the HG_{11}, HG_{21}, LG_{10}, and LG_{11} beams.

Reference

1) T. Kuga, Y. Torii, N. Shiokawa, T. Hirano, Y. Shimizu and H. Sasada, *Phys. Rev. Lett.* **78**, 4713 (1997).

II-F Ultrafast Dynamics of Surface Adsorbed Species

Understanding of reaction dynamics at surfaces using ultra-short laser techniques is an important issue to clarify the mechanism of the reactions. Real-time observation of temporal change of surface species induced by UV, visible, and (Near-) infrared pump pulses is carried out using mid-IR pump-probe vibrational spectroscopy and Sum-frequency generation (SFG) spectroscopy which is one of the non-linear spectroscopies using ultra-short laser has high sensitivity for detection of molecular vibrations of adsorbed species on surface in the first layer. The aim of this study is the identification of molecular structures of the intermediates generated by electronic, vibrational, or thermal excitation and understanding of the reaction kinetics including potential energies, activation barriers, and entropies. Typical systems of our recent studies are formate (DCOO) adsorbed on Ni(111) surface, CO on Ni(111) surface, and D_2O on OD groups in alumina.

II-F-1 Time-Resolved Study of Formate on Ni(111) by Picosecond SFG Spectroscopy

KUSAFUKA, Koji[1]; ONDA, Ken[1]; NOGUCHI, Hidenori[1]; KUBOTA, Jun[1]; DOMEN, Kazunari[1]; HIROSE, Chiaki[1]; WADA, Akihide[2]
([1]Tokyo Inst. Tech.; [2]IMS and Tokyo Inst. Tech.)

[*Surf. Sci.* **502/503**, 313 (2002)]

Time-resolved vibrational measurements were carried out on formate (HCOO) adsorbed on Ni(111) surface by combining the sum-frequency generation (SFG) method and picosecond laser system (time-resolution of 6 ps). Rapid intensity decrease (within the time-resolution) followed by intensity recovery (time-constant of several 10s ps) of CH stretching signal was observed when picosecond 800 nm pulse was irradiated on the sample surface. From the results of temperature and pump fluence dependences of temporal behaviour of signal intensity, we concluded that the observed intensity change was induced by non-thermal process. Mechanism of the temporal intensity change was discussed.

II-F-2 SFG Spectroscopy of CO/Ni(111): UV Pumping and Transient Hot Band Transition of Adsorbed CO

BANDARA, Athula[1]; KANO, Satoru S.[2]; ONDA, Ken[1]; KATANO, Satoshi[1]; KUBOTA, Jun[1]; DOMEN, Kazunari[1]; HIROSE, Chiaki[1]; WADA, Akihide[3]
([1]Tokyo Inst. Tech,; [2]Hosei Univ.; [3]IMS and Tokyo Inst. Tech.)

[*Bull. Chem. Soc. Jpn.* **75**, 1125 (2002)]

A UV excitation by a picosecond pulse at 266 nm induced an unusual shoulder to the $\nu_{CO} = 1 \leftarrow 0$ resonance peak of CO/Ni(111) monitored by sum-frequency generation (SFG) of visible and IR pulses. The observed line shape was reproduced by the use of a dipole-dipole interaction model with the coherent potential approximation (CPA) where the hot band transition with a population ratio of 0.3 to 0.7 ($v = 1$ to $v = 0$) was assumed. Neither the transition to the two-phonon bound state nor the coupling with the low-frequency phonon modes explained the observed changes. The shoulder appeared only during the UV excitation, which indicated that the electronically driven excitation, presumably by the hot electrons generated by the irradiation, dominated the process. As possible mechanisms, the involvement of intermediate negative ion resonance state and/or the non-adiabatic coupling of electronic states with C–O stretching mode were considered.

II-F-3 Surface Hydroxyl Group and Adsorbed Water on γ-Al_2O_3 Studied by Picosecond Infrared Pump-Probe Experiment

ONDA, Ken[1]; TANABE, Kinuka[1]; NOGUCHI, Hidenori[1]; WADA, Akihide[3]; SHIDO, Takahumi[2]; YAMAGUCHI, Aritomo[2]; IWASAWA, Yasuhiro[2]
([1]Tokyo Inst. Tech., [2]Univ. Tokyo; [3]IMS and Tokyo Inst. Tech.)

[*J. Phys. Chem. B* **105**, 11456 (2001)]

Picosecond infrared-infrared pump-probe experiments in the OD stretching region were carried out on dehydrated and multilayer water-adsorbed γ-Al_2O_3. For the dehydrated γ-Al_2O_3, transient bands assigned to the bleaching and hot bands of the OD stretching mode of isolated surface hydroxyl groups were observed, and the population lifetime (T_1) of the vibrational excited state ($v = 1$) of the mode was 200 ± 10 ps at 293 K. The characteristic temperature dependence of T_1 is indicative of a seven-phonon process. For the water-adsorbed γ-Al_2O_3, the transient bleaching and transient hot bands with a lifetime of 10–12 ps were observed by excitation of the absorption peak at 2630 cm^{-1}. In addition to these bands, weak transient bands were observed in the low frequency region. These results are considered evidence of the existence of isolated water molecules on the γ-Al_2O_3 surface. Pure dephasing is also discussed based on the bandwidth of the observed transient bands.

II-G Spin Reorientation Transitions of Ultrathin Magnetic Films Induced by Chemisorption

Magnetic anisotropy of ultrathin metal films is one of the most attractive subjects in magnetism. When one considers magnetic anisotropy of thin films within the framework of the classical electromagnetic theory, one finds that in-plane magnetization is always more stable than perpendicular magnetization. Perpendicular magnetic anisotropy (PMA) is, however, sometimes observed in real systems and the understanding of the origin of PMA is important from the viewpoints of both fundamental physics and technological applications to new-generation high-density recording media. We have been investigating the microscopic mechanism of PMA that is stabilized by gaseous adsorption on magnetic film surfaces by means of the synchrotron radiation x-ray magnetic circular dichroism (XMCD) technique. A goal of these works is spin engineering by which the magnetization of ultrathin metal films can be controlled artificially.

II-G-1 Perpendicular Magnetic Anisotropy in Co/Pd(111) Stablized by Chemisorption of CO and NO

YOKOYAMA, Toshihiko; MATSUMURA, Daiju[1]; AMEMIYA, Kenta[1]; KITAGAWA, Soichiro[1]; SUZUKI, Norihiro[1]; OHTA, Toshiaki[1]
([1]Univ. Tokyo)

[*J. Phys.: Condens. Matter* in press]
[*Phys. Rev. B* **66**, 024402 (2002)]

Spin reorientation transitions of ultrathin Co/Pd(111) films induced by adsorption of atoms and molecules have been investigated by means of Co $L_{III,II}$-edge x-ray magnetic circular dichroism (XMCD). We have examined CO, NO, O and H as chemisorbed species. Figures 1(a) and 1(b) show the Co $L_{III,II}$-edge XMCD spectra on clean and CO-adsorbed 4.5 ML Co/Pd(111) at 200 K, respectively. In clean Co/Pd(111) [Figure 1(a)] the XMCD signal appears only in the grazing-incidence (θ = 30˚) spectrum, while in CO-adsorbed Co/Pd(111) the normal-incidence (θ = 90˚) spectrum gives a two-times more intense XMCD signal than the θ = 30˚ spectrum. These observation directly implies that the magnetization direction varies from in-plane to perpendicular upon CO adsorption. We observed a similar adsorbate-induced spin reorientation transition in the NO case as well, while in O or H adsorption no transitions took place. We have investigated detailed Co-thickness dependence in the case of CO. Figures 1(c) and 1(d) show the Co spin magnetic moments of clean and CO-adsorbed Co/Pd(111), respectively. The critical thickness of the spin reorientation transition in CO-adsorbed Co is found to be ~6.5 ML, which is by ~3 ML greater than that of clean Co (~3.5 ML), implying the stabilization of PMA by CO adsorption.

The most important information from XMCD is the orbital magnetic moments, which determine the magnetic easy axis in spite of very small contribution to the total magnetic moments. Figure 1(e) shows the orbital magnetic moments of Co on clean and CO-adsorbed Co/Pd(111). Below ~3.5 ML the *surface normal* orbital moment is found to be left *unchanged*, while above ~6.5 ML the *surface parallel* orbital moment is *reduced* significantly after CO adsorption. We conclude that the observed stabilization of perpendicular magnetic anisotropy due to adsorption is ascribed to *quenching* of the *surface parallel orbital* magnetic moment.

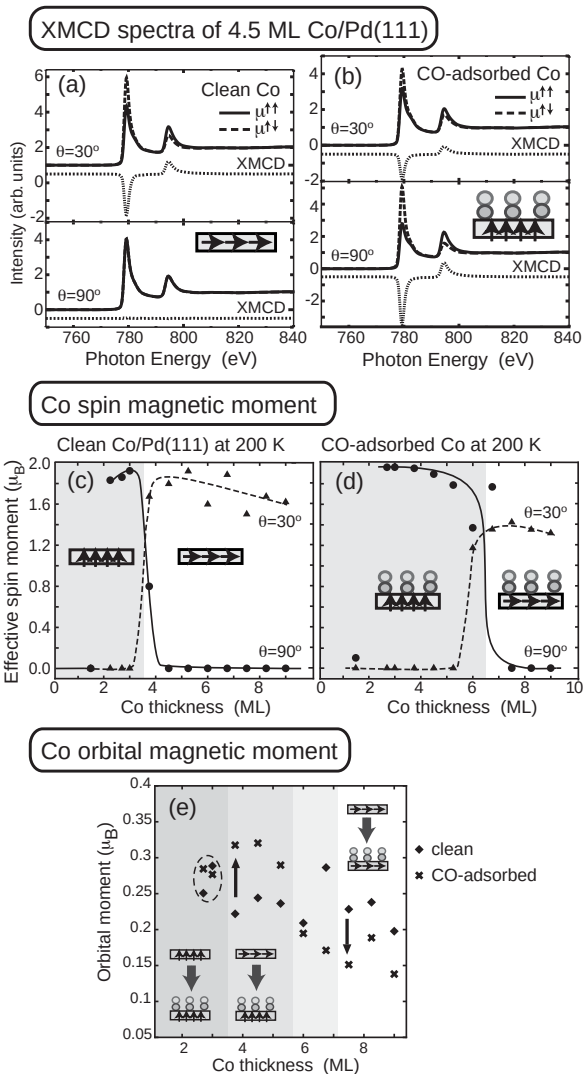

Figure 1. (a), (b): Co $L_{III,II}$-edge circularly polarized (solid and dashed lines) and XMCD (dotted line) spectra of 4.5 ML Co/Pd(111) at 200 K before (a) and after (b) CO adsorption. θ is the angle between surface normal and the x-ray electric field (θ = 30˚ and θ = 90˚ correspond to grazing and normal x-ray incidence, respectively). It is found that the magnetic easy axis rotates from in-plane in (a) to perpendicular in (b).

(c), (d): Co thickness dependence of the Co spin magnetic moments at 200 K. Hatched areas indicate the PMA regions. The critical thickness for the spin reorientation transition is ~3.5 ML for clean Co (c) and ~6.5 ML for CO-adsorbed Co (d), this indicating that the perpendicular magnetic anisotropy is stabilized upon CO adsorption.

(e): Co thickness dependence of the Co orbital magnetic moments at 200 K. After CO adsorption, the perpendicular orbital moment does not vary so much (see the data below ~3.5 ML), while the in-plane orbital moment reduces significantly (see the ones above ~ 7 ML).

II-H Local Structures in Photoinduced States of Molecular-Based Magnetic Materials

Molecular-based magnets provide noble properties such as photoinduced magnetism. Photoinduced phase transition is closely related to bistability of the ground state in the material. Light irradiation stimulates the macroscopic phase transition between the ground state and the metastable state, although thermal fluctuation triggers the thermal phase transition. Although it has been believed that the photoinduced phase is the same state as the thermally induced phase, recent investigations have reported some differences in structure from the high-temperature phase. We have been studying local structures and electronic properties of photoinduced phases of Prussian-blue analogues and other metal-complex magnets by means of x-ray absorption fine structure (XAFS) spectroscopy. XAFS is one of the most suitable methods for these purposes since the technique does not require long-range order in the sample and provide element-specific information about each metal atom.

II-H-1 Photoinduced Phase Transition of $RbMnFe(CN)_6$ Studied by X-Ray-Absorption Fine Structure Spectroscopy

YOKOYAMA, Toshihiko; TOKORO, Hiroko[1]; OHKOSHI, Shin-ichi[1]; HASHIMOTO, Kazuhito[1]; OKAMOTO, Kaoru[1]; OHTA, Toshiaki[1]
([1]Univ. Tokyo)

[*Phys. Rev. B* **66**, 184111 (2002)]

A Prussian-blue analogue of $RbMnFe(CN)_6$ shows a thermally induced first-order phase transition ($T_{c\downarrow}$ = 231 K and $T_{c\uparrow}$ = 304 K) and also turns to a ferromagnetic phase below 12 K. Upon visible-light irradiation, the ferromagnetism is quenched and the phase is transformed to the metastable nonmagnetic state. In this work, we have investigated the photoinduced magnetic phase transition of $RbMnFe(CN)_6$ by means of XAFS spectroscopy.

Mn and Fe *K*-edge x-ray-absorption near-edge structure spectra have clarified that upon the phase transition, a Fe 3*d* electron is transferred to the Mn 3*d* level; the electronic state of Mn changes from trivalent (d^4, spin momentum S = 2) to divalent (d^5, S = 5/2), while the Fe state correspondingly varies from divalent (d^6, S = 0) to trivalent (d^5, S = 1/2). Such a tautomeric scheme in the photoinduced phase transition is exactly the same as in the thermally induced transition.

Local structures have been investigated by the extended x-ray-absorption fine-structure analysis for the photoinduced phase as well as for the low- and high-temperature phases. The low-temperature phase shows a significant Jahn-Teller distortion in the Mn(III) octahedron, where the Mn–N distances for four shorter and two longer bonds are 1.964 ± 0.008 Å and 2.21 ± 0.01 Å, respectively. The high-temperature phase gives a longer Mn–N distance of 2.211 ± 0.006 Å, although some minor contribution from a shorter distance still remains. It is also revealed that the atomic configuration of the –Fe–C–N–Mn– chain is essentially collinear and that the Rb ions locate at the center of the cubic lattice. The photoinduced phase was found to be structurally and electronically identical to the high-temperature phase. Summary of the present investigation is given in Figure 1.

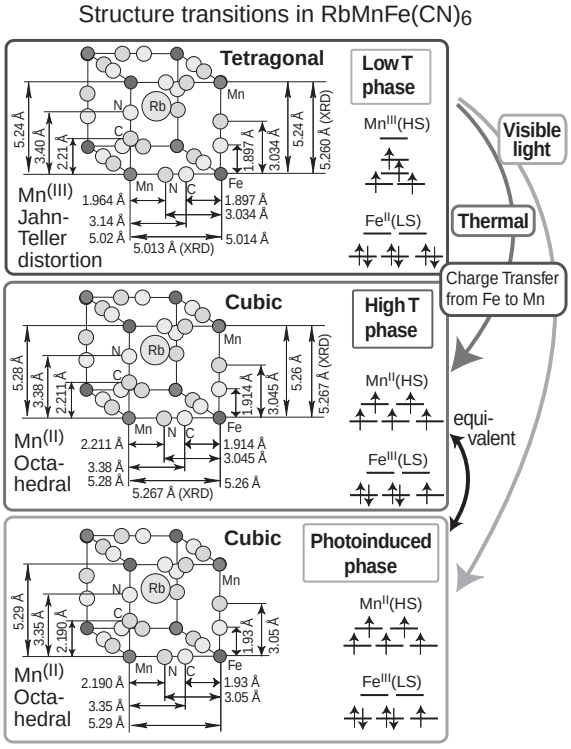

Figure 1. Summary of the present investigation for the phase transitions in $RbMnFe(CN)_6$.

II-I Molecular and Electronic Structures of Metallofullerenes

The continued interest in radical ions of fullerenes and metallofullerenes has resulted from the discovery of superconductivity in the CT complexes of alkali metals with fullerenes. Spectroscopic information concerning the electronic and spin states of the metallofullerenes has been obtained by ESR measurements.

II-I-1 Spin Dynamics of Lanthanum Metallofullerenes

OKUBO, Shingo; KATO, Tatsuhisa

Full separation of topological isomers of each La@C_n component (n = 76 to 90) was attempted by 2-stage HPLC separation with chlorobenzene eluent, and all species of La@C_n with even number n from 76 to 90 were detected. Their Electron Spin Resonance (ESR) spectra were recorded at various temperatures. The line width of the ESR spectrum in CS_2 solution was analyzed by the theory on the basis of hydrodynamics. Enormous variety of ESR spectra of La@C_ns was obtained in terms of g factor, hyperfine coupling constant, and line width. The feature of the temperature dependence of the line width was almost interpreted by the hydrodynamics, and the electronic structure of La@C_n was deduced from the ESR parameters. However in the cases of the isomer I of La@C_{80} and isomer II of La@C_{84} abnormally large line width was measured, as shown in Figure. The topological cage structure of La@C_{80} and La@C_{84} reflected on the specific spin dynamics.

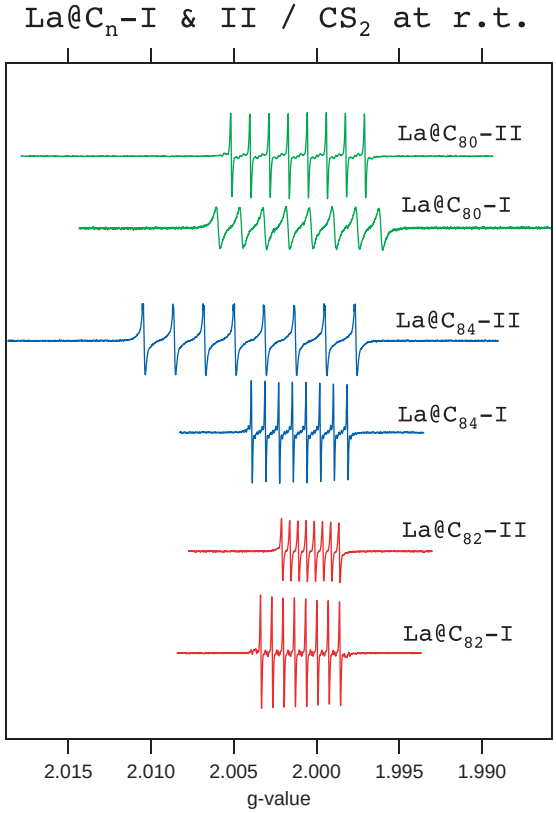

Figure 1. X-band ESR spectra of both isomers I and II of La@C_{80}, La@C_{82}, and La@C_{84} in CS_2 solution.

II-I-2 Electronic State of Scandium Trimer Encapsulated in C_{82} Cage

KATO, Tatsuhisa; OKUBO, Shingo; SHINOHARA, Hisanori[1]
([1]Nagoya Univ.)

The ESR spectrum of Sc_3@C_{82} in toluene and CS_2 solutions exhibits the symmetric hyperfine splitting of the 22 lines with a line width of 0.5 gauss at room temperature, which was consistent with the structure of Sc_3@C_{82} having the C_{3v} symmetry. The line widths of the 22 lines were much broader than that for Sc@C_{82}. The broader line width of the scandium trimmer in C_{82} could reflect the intra-molecular dynamics that averaged among three Sc metals' environments in the Jahn-Teller distorted structure of the whole molecule. The intra-molecular dynamics is the inherent nature of the Sc trimer encapsulated in the C_{82} cage with the symmetry of C_{3v}. The intra-molecular charge transfer from the central metal to the fullerene cage would give the stable electronic structure of an endo-metallofullerene. The X-ray diffraction study reported that there was no bonding electron between the cage and the trimmer, and that the charge state of the Sc_3 was 3+ leading to the electronic structure of $(Sc_3)^{3+}$@C_{82}^{3-}. Electron spin resonance (ESR) spectrum of the scandium trimmer encapsulated in the C_{82} cage (Sc_3@C_{82}) was measured at the low temperature. The spectrum exhibited the specific pattern due to the strongly an-isotropic hyperfine tensor of the scandium trimmer. The electronic state of the Sc_3@C_{82} was given from the analysis of the hyperfine tensor, as shown in Figure 1.

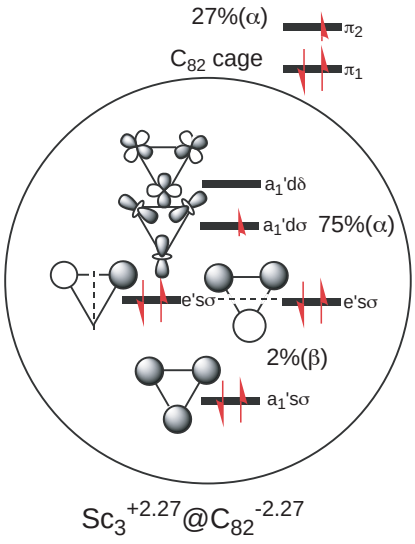

Figure 1. The Electronic structure of Sc_3@C_{82} molecule deduced from the analysis of the hyperfine tensor of Sc metal.

II-I-3 Efficient Reduction of Metallofullerenes by Solvation of Pyridine and Dimethylformamide

OKUBO, Shingo; KATO, Tatsuhisa; MAEDA, Yutaka[1]; AKASAKA, Takeshi[1]
([1]Univ. Tsukuba)

Various solvents have been used in the extraction of endohedral metallofullerenes from the raw soot produced by the arc-discharge method. Toluene, CS_2, and chlorinated benzenes have been used generally as solvent. On the other hand, pyridine and dimethylformamide (DMF) are known to give effective enrichment of metallofullerenes in the extraction, and aniline is especially effective for endohedral metallo-C_{60}. The specific affinity of these solvents with metallofullerenes would be attributed to the electronic interaction of the lone pair electron on nitrogen of the solvent with the π orbital of the metallofullerene's cage. However the exact nature of the interaction has not been clarified as yet. We recently presented the evidence that anions of La@C_{82}-I and Gd@C_{82}-I are easily produced with almost 100% yield by the solvation of pyridine and DMF. The formation of the La@C_{82}-I anion was confirmed by Vis-NIR and ^{13}C-NMR measurements, which gave identical spectra with those of the La@C_{82}-I anion reported before. The ^{139}La-NMR and ^{13}C-NMR spectra of La@C_{82}-I anion are respectively shown in Figure. The chemical shift of the ^{139}La-NMR line corresponded with that reported before. For assignment the anion generated in DMF, ^{13}C-NMR spectrum was measured under same condition of electrochemically method in literature. After addition of electrolyte (TBAP) and removed DMF, the anion of La@C_{82} generated in DMF was dissolved in a mixture of CS_2 and acetone (1:1). The spectrum is in good agreement with that prepared by electrochemical method. The electron spin resonance (ESR) and Vis-NIR spectra of Gd@C_{82}-I dissolved in pyridine and DMF also give good agreements with those of the anion produced by electrochemical reduction. It could be generally concluded that the solvation of pyridine, and DMF, and aniline leads to the efficient reduction of endohedral metallofullenes.

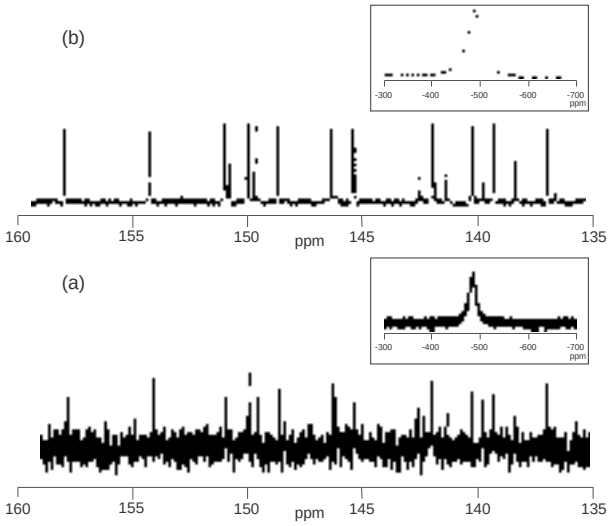

Figure 1. ^{139}La-NMR spectrum of La@C_{82}-I recorded in the DMF-d7 solution (a) and that of the La@C_{82}-I anion produced by electrochemistry (b), as shown in the inset of Figure. ^{13}C-NMR spectrum of La@C_{82}-I in DMF (a) was measured under same condition of electrochemically method (b) in literature.

II-J High Field and Pulsed Electron Spin Resonance Spectroscopy

Electron spin resonance (ESR) spectroscopy has been a powerful technique for the characterization of radical species. The modern development of EPR spectroscopy enables us to investigate the heterogeneous and disordered system in detail. Especially the high frequency and pulsed EPR methods achieve the substantial resolution enhancement of spectrum. The advanced EPR spectroscopy is applied to study on the reaction mechanism in the heterogeneous system and the detection of the multi-cation species.

II-J-1 High-Field/High-Frequency ESR Study of Gadolinium Metallofullerenes

FURUKAWA, Ko; TOYAMA, Namiki; OKUBO, Shingo; KATO, Tatsuhisa

A high-field/high-frequency ESR spectrometer is a powerful means to determine the complicated spin state of metallofullerenes. The analysis of the spin states of Gd@C_{82}-I and related species are reported here. The electronic structure of a gadolinium metallofullerene is stabilized by the intra-molecular charge transfer, and is described by the electronic configuration of Gd($4f^7$)-@C_{82}(π^1), as shown in the Figure 1. The complicated electron spin state would be expected because of the combination of the octet spin site of gadolinium with the π spin of the fullerene cage. If the exchange interaction of J between the π spin and the octet spin is negative, these spins couple in anti-ferromagnetic manner and the resultant spin quantum number S will be 3. If the π spin on the cage is cancelled by adding an extra spin on the π orbital, S will be 7/2. This cancellation would be attained in the case of Gd@C_{82} anion, or in the case of the dimmerization of two Gd@C_{82}s. The π spin on the cage has the key function for the determination of the total spin state, and we confirmed the spin

state of Gd@C_{82}-I in its monomer form, dimmer form, and anion form by the high-field/high-frequency ESR measurement as shown in Figure 1.

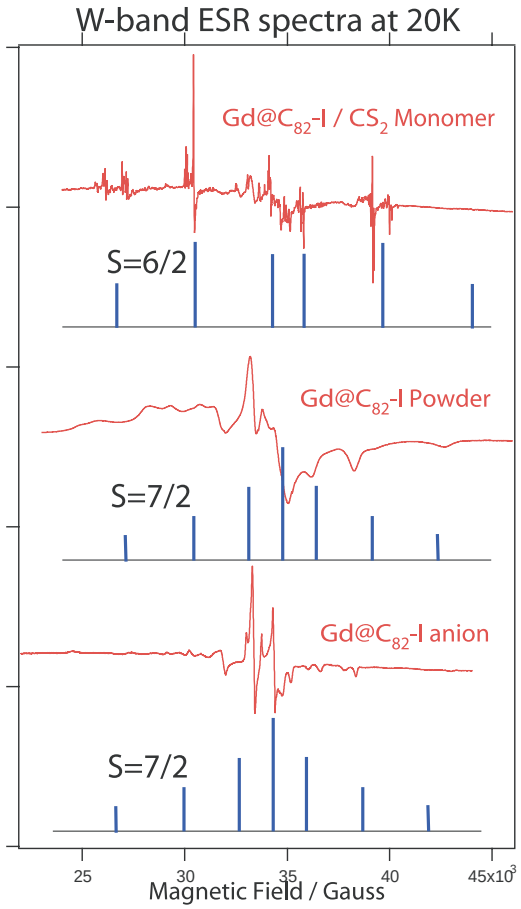

Figure 1. The high-field/high-frequency ESR (95 GHz) spectra of Gd@C_{82}-I in its monomer form, dimmer form, and anion form produced by the electrochemical method.

II-J-2 A Bindschedler's Green-Based Arylamine: Its Polycations with High-Spin Multiplicity

KANEMOTO, Katsuichi; KATO, Tatsuhisa; ITO, Akihiro[1]; INO, Haruhiro[1]; MATSUI, Yuki[1]; TANAKA, Kazuyoshi[1]
([1]Kyoto Univ.)

Intramolecular high-spin correlation in a series of the successively generated polycationic species of Bindschedler's green-based arylamine, *N*,*N*,*N*',*N*',*N*",*N*"-hexakis[4-(dimethylamino)phenyl]-1,3,5-benzenetriamine (**1**) have been investigated by continuous and pulsed EPR spectroscopy. Cyclic voltammetry shows multi-redox behavior of **1** that can be reversibly oxidized from monocation to hexacation. Depending on quantity of the added oxidant, the characteristic EPR spectra are observed for polycations of **1** in frozen solution. Unequivocal determination of the spin state at each oxidation stage of **1** is given by a pulse EPR technique, that is, electron spin transient nutation spectroscopy as shown in Figure 1. Observation of the unusual spin state after annealing of the highly charged polycations of **1** is also reported.

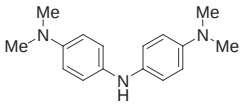

BG leuco base

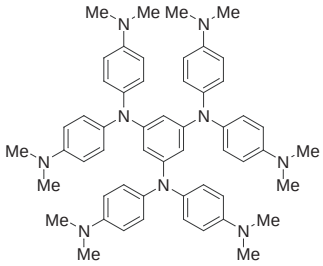

1

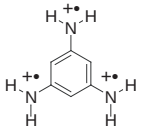

BTA^{3+}

Scheme 1. (**1**): Molecular structures of *N*,*N*,*N*',*N*',*N*",*N*"-hexakis [4-(dimethylamino) phenyl]-1,3,5-benzenetriamine.

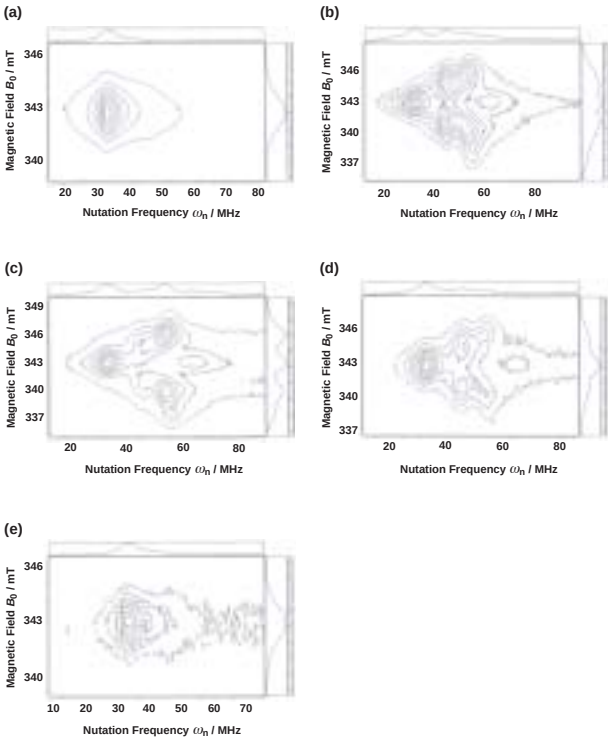

Figure 1. Field-swept electron spin transient nutation spectra of **1** oxidized by (a) 1 molar equiv, (b) 2 molar equiv, (c) 3 molar equiv, (d) 4 molar equiv, and (e) 5 molar equiv of TBA·$SbCl_6$ in *n*butyronitrile at 5 K. ω_1 corresponds to about 30 MHz.

II-K State Correlated Raman Spectroscopy

The vibrational Raman polarizability tensor responds to molecular reorientational relaxation process, and the structural environment in condensed media. The measurement of Raman scattering is a powerful technique for the study of molecular motion and of the mechanism of phase transition. We've built up the system of multichannel type detection of Raman scattering combined with the temperature controlled cell.

II-K-1 Molecular Ordering Deformation Induced by Externally Applied Electric Field in an Antiferroelectric Liquid Crystal

HAYASHI, Naoki; KATO, Tatsuhisa; ANDO, Tomohiro[1]; FUKUDA, Atsuo[1]
([1]Shinshu Univ.)

[*Jpn. J. Appl. Phys.* **41**, 5292 (2002)]

Molecular orientational ordering in an antiferroelectric liquid crystal was studied by observing polarized Raman scattering in a homogeneously aligned thin sample exposed to static electric field. The apparent orientational order parameters gradually increased with the applied electric field strength even in the pretransitional regime from antiferro- to ferroelectric phase although the averaged molecular orientation was hardly changed. (See Figure 1) This change in the order parameters indicates the deformation of the *c*-director and is represented by the similar equation describing the nematic director deformation induced by an external electric field, in which the electric coherence length was inversely proportional to the applied electric field strength.

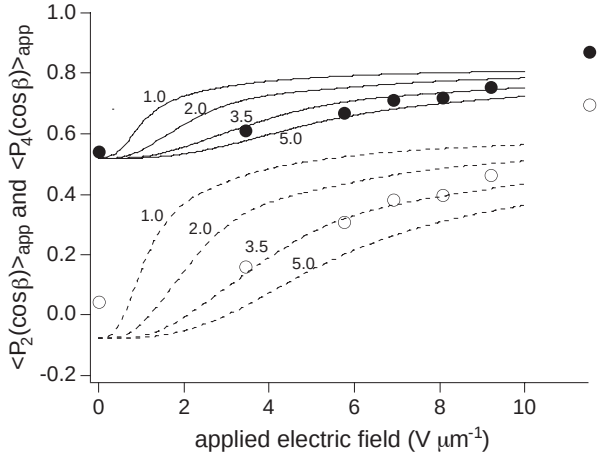

Figure 1. Apparent orientational order parameters under static electric field, solid circle: $\langle P_2(\cos\beta)\rangle_{app}$; open circle: $\langle P_4(\cos\beta)\rangle_{app}$. The solid and dotted lines are $\langle P_2(\cos\beta)\rangle_{app}$ and $\langle P_4(\cos\beta)\rangle_{app}$ given by the model calculation. The numbers beside the lines show the values of $\xi_b E$; 1.0, 2.0, 3.5 and 5.0 V. Here, ξ_b is the electric coherence length and E is the applied electric field strength.